estimate the Reynolds number for the cases High and High-S. The values are 2000 and 7000 for the cases High and High-S, respectively (the detailed explanation for the estimation is given in the supplementary materials). Thus, the effective diffusivities for the cases High and High-S are 1.6×10^{11} and 4.6×10^{10} cm^2 s^{-1}, respectively. Because it was found in (*23*) that the critical Reynolds number for exciting the dynamo is ~100, our achieved Reynolds numbers are ~20 and 70 times larger than the threshold. Although the presented calculation has still a much larger viscosity and magnetic diffusivity than those of the real Sun ($< 10^4$ cm^2 s^{-1}), the obtained mechanism does not require any assumption of large "turbulent" diffusivities because Maxwell stresses from the small-scale field can mimic their effect.

REFERENCES AND NOTES

1. I. G. Usoskin, K. Mursula, G. A. Kovaltsov, *Sol. Phys.* **218**, 295–305 (2003).
2. G. E. Hale, S. B. Nicholson, *Astrophys. J.* **62**, 270 (1925).
3. E. N. Parker, *Astrophys. J.* **122**, 293 (1955).
4. M. Ghizaru, P. Charbonneau, P. K. Smolarkiewicz, *Astrophys. J.* **715**, L133–L137 (2010).
5. B. P. Brown, M. S. Miesch, M. K. Browning, A. S. Brun, J. Toomre, *Astrophys. J.* **731**, 69 (2011).
6. Y. Fan, F. Fang, *Astrophys. J.* **789**, 35 (2014).
7. N. J. Nelson, B. P. Brown, A. S. Brun, M. S. Miesch, J. Toomre, *Astrophys. J.* **762**, 73 (2013).
8. S. M. Tobias, F. Cattaneo, *Nature* **497**, 463–465 (2013).
9. F. Cattaneo, S. M. Tobias, *Astrophys. J.* **789**, 70 (2014).
10. S. Chapman, *Astrophys. J.* **120**, 151 (1954).
11. T. G. Cowling, "Solar Electrodynamics," in *The Sun*, G. P. Kuiper, Ed. (Univ. Chicago Press, Chicago, 1953), pp. 532–591.
12. H. Hotta, M. Rempel, T. Yokoyama, *Astrophys. J.* **803**, 42 (2015).
13. H. Hotta, M. Rempel, T. Yokoyama, Y. Iida, Y. Fan, *Astron. Astrophys.* **539**, A30 (2012).
14. J. Christensen-Dalsgaard *et al.*, *Science* **272**, 1286–1292 (1996).
15. H. Hotta, M. Rempel, T. Yokoyama, *Astrophys. J.* **786**, 24 (2014).
16. H. Hotta, M. Rempel, T. Yokoyama, *Astrophys. J.* **798**, 51 (2015).
17. A. Kageyama, T. Sato, *Geochem. Geophys. Geosyst.* **5**, 9005 (2004).
18. M. Rempel, *Astrophys. J.* **789**, 132 (2014).
19. M. J. Thompson, J. Christensen-Dalsgaard, M. S. Miesch, J. Toomre, *Annu. Rev. Astron. Astrophys.* **41**, 599–643 (2003).
20. T. Gastine, R. K. Yadav, J. Morin, A. Reiners, J. Wicht, *Mon. Not. R. Astron. Soc.* **438**, L76–L80 (2014).
21. N. A. Featherstone, M. S. Miesch, *Astrophys. J.* **804**, 67 (2015).
22. B. P. Brown, M. K. Browning, A. S. Brun, M. S. Miesch, J. Toomre, *Astrophys. J.* **711**, 424–438 (2010).
23. A. S. Brun, M. S. Miesch, J. Toomre, *Astrophys. J.* **614**, 1073–1098 (2004).

ACKNOWLEDGMENTS

We are grateful to M. Miesch, R. Cameron, and M. Schüssler for helpful comments. H.H. is supported by a Japan Society for the Promotion of Science Postdoctoral Fellowship for Research Abroad. The National Center for Atmospheric Research is sponsored by the National Science Foundation. The results were obtained by using the K computer at the RIKEN Advanced Institute for Computational Science (Proposal no. hp140212 and hp150226) and the Yellowstone Supercomputer at NCAR (project code NHA00005). This work was supported by the Ministry of Education, Culture, Sports, Science and Technology Strategic Programs for Innovative Research, Joint Institute for Computational Fundamental Science, and Project for Solar-Terrestrial Environment Prediction. Statistical data from the calculations and executable software are available in the supplementary materials.

SUPPLEMENTARY MATERIALS

www.sciencemag.org/content/351/6280/1427/suppl/DC1
Supplementary Text
Table S1
Figs. S1 to S5
References (*24*–*26*)
Movie S1
Calculation result in IDL format (science.idl)
Executable file compiled with Fujitsu Fortran

5 August 2015; accepted 10 February 2016
10.1126/science.aad1893

SOLAR CELLS

Photon recycling in lead iodide perovskite solar cells

Luis M. Pazos-Outón,[1] Monika Szumilo,[1] Robin Lamboll,[1]* Johannes M. Richter,[1]* Micaela Crespo-Quesada,[2] Mojtaba Abdi-Jalebi,[1] Harry J. Beeson,[1] Milan Vrućinić,[1] Mejd Alsari,[1] Henry J. Snaith,[3] Bruno Ehrler,[4] Richard H. Friend,[1]† Felix Deschler[1]†

Lead-halide perovskites have emerged as high-performance photovoltaic materials. We mapped the propagation of photogenerated luminescence and charges from a local photoexcitation spot in thin films of lead tri-iodide perovskites. We observed light emission at distances of ≥50 micrometers and found that the peak of the internal photon spectrum red-shifts from 765 to ≥800 nanometers. We used a lateral-contact solar cell with selective electron- and hole-collecting contacts and observed that charge extraction for photoexcitation >50 micrometers away from the contacts arose from repeated recycling between photons and electron-hole pairs. Thus, energy transport is not limited by diffusive charge transport but can occur over long distances through multiple absorption-diffusion-emission events. This process creates high excitation densities within the perovskite layer and allows high open-circuit voltages.

Since 2009 (*1*), hybrid lead halide perovskite photovoltaics have shown a marked rise in power conversion efficiency to values that are almost comparable to that of crystalline silicon (*2*–*7*). This improved photovoltaic performance has been attributed to well-suited material properties such as high absorption cross sections (*8*), long charge-carrier lifetimes (*9*), and high emission yields (*10*). Recent studies in single crystals have reported charge diffusion lengths of 175 μm (*11*, *12*); in polycrystalline thin films, vertical diffusion lengths have been found to be longer than 1 μm (*13*, *14*). Together with high radiative recombination yields and long carrier lifetimes, these properties raise the question of whether absorption and reemission of excited carriers can occur during the transport. We report that such "photon recycling" does indeed play a central role, allowing considerable increases over current descriptions in the characteristic lengths for charge and energy transport.

Highly crystalline inorganic semiconductors with high internal quantum yields, such as GaAs, demonstrate the current record efficiencies in single-junction solar cells (*15*, *16*). The low nonradiative recombination rates and high photoluminescence (PL) yields of these materials allow one photoexcited state to undergo multiple radiative emission-absorption events before it is lost through nonradiative decay (*17*, *18*). This photon recycling effect, together with photonic confinement caused by the difference in refractive index between the active material and its surroundings, leads to a buildup of excited-state population in the bulk of the material, similar to a solar concentration effect (*17*). Additionally, the length scales for energy transport are not limited to a single charge diffusion length but can occur through multiple recombination-emission events in an interchange between light and charge states, which markedly enhances the transport length scales.

Previous studies of lead iodide perovskites have shown a sharp absorption onset at the optical band edge, with an Urbach tail slope close to that of GaAs (*8*, *19*), whereas the PL spectrum is homogeneously broadened by interaction with phonons, leading to a considerable intensity beyond the band edge (*20*). Additionally, long carrier lifetimes and low nonradiative losses have been reported (*9*, *10*). These conditions could support photon recycling.

We studied thin perovskite films (with a thickness of ~100 nm) on glass substrates [details of preparation and characterization can be found in the supplementary materials (*21*)]. Under these conditions, only 10 to 15% of internally generated PL escaped to the air above or to the glass below [calculation in the supplementary materials (*21*)], and the remaining emission was guided within the film (*22*). To measure the spatial distribution of photogenerated emission, we used a confocal optical microscope setup with separately controlled excitation and collection objectives and a spatial resolution of ~1.5 μm (Fig. 1A and fig. S1) (*21*). Photons propagating in the film could be scattered out of the film or be absorbed and re-emitted isotropically. We measured the emission from the edge of the film, maximizing outscattering and allowing the detection of both components. These results provide a direct probe of the internal photon distribution traveling through the film. Figure 1B shows spatial emission mapping. When excitation is near the edge (≤4 μm), the observed spectrum is similar to the macroscopic PL of this film, centered at ~765 nm (Fig. 1C). However, when the excitation objective was moved farther away from the collection spot, the internal spectrum continuously red-shifted to

[1]Cavendish Laboratory, University of Cambridge, JJ Thomson Avenue, CB3 0HE Cambridge, UK. [2]Department of Chemistry, University of Cambridge, CB2 1EW Cambridge, UK. [3]Clarendon Laboratory, Department of Physics, University of Oxford, OX1 3PU Oxford, UK. [4]Center for Nanophotonics, FOM Institute AMOLF, Science Park 104, 1098 XG Amsterdam, Netherlands.
*These authors contributed equally to this work. **†Corresponding author. E-mail: rhf10@cam.ac.uk (R.H.F.); fd297@cam.ac.uk (F.D.)**

beyond 800 nm after the separation increased to 50 μm. Unexpectedly, at these distances we still detected a blue (765-nm) component in the spectrum at a wavelength similar to those of the initial emission spectrum, the origin of which we discuss below.

We used photothermal deflection spectroscopy to measure the absorption coefficients α_λ (where λ is the wavelength) of the films and then compared our findings with the photoluminescence excitation spectrum (Fig. 1C). Under conditions in which photons are mostly confined within a slab (formed here by the glass-perovskite-air structure), the Beer-Lambert law gives a decay in spectral photon population I_λ away from a pointlike excitation spot with radius r_0

$$I_\lambda(r) = \frac{r_0}{r} I_{\lambda_0} \cdot e^{-(\alpha_\lambda \cdot r)} \quad (1)$$

This relation indicates that the decay is monoexponential for each wavelength, with an additional radial factor. Using Eq. 1, the predicted spectral decay map following this law is plotted in Fig. 1D. The measured decay in the different spectral regions was substantially slower than the prediction from the Beer-Lambert law. To illustrate the difference, the decay for selected wavelengths was extracted (Fig. 1E) and compared with Beer-Lambert predictions. Beer-Lambert predictions do not take scattering into account, which further accelerates the decay, particularly in spectral regions of very low absorption.

We attribute the main red-shifted peak to guided photons that out-scattered at the edge of the film. Scattering is nondispersive, so we expect these out-scattered photons to match the internal spectral distribution of photons travelling inside the film. The internal photon spectral distribution was biased toward longer-wavelength photons that travelled farther between emission and absorption events due to the sharp decay of the absorption coefficient at the band tail. These

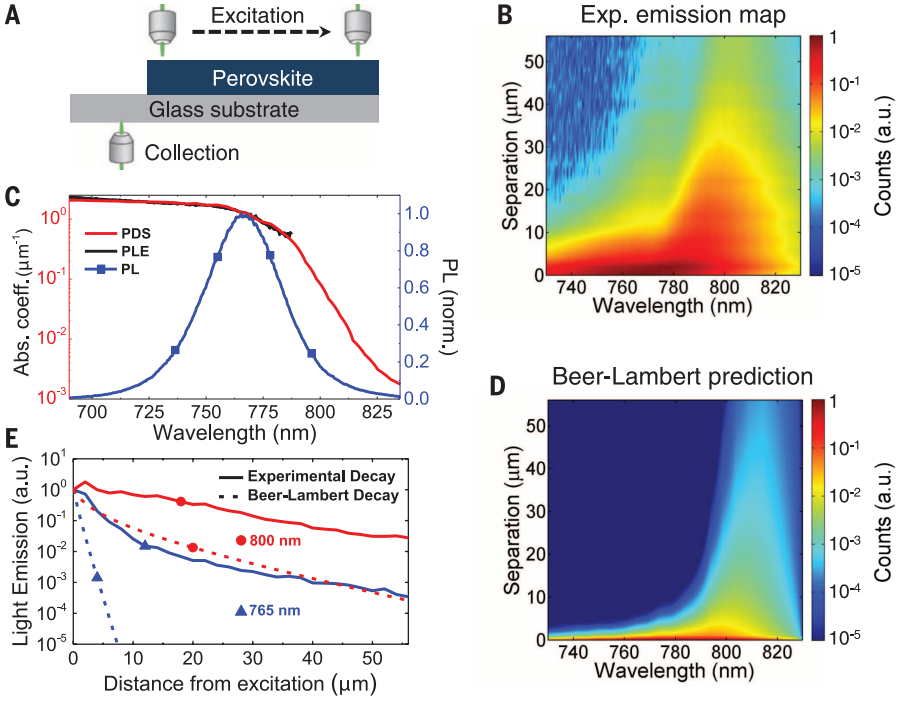

Fig. 1. Spatial mapping of emission and photon spectrum. (**A**) Graphical representation of microscope setup and measurement geometry. (**B**) Experimentally measured light emission map for different separation distances between excitation and collection. (a.u., arbitrary units) (**C**) Comparison of normalized PL with PL excitation (PLE) and photothermal deflection spectra. (**D**) Predicted spatial light emission spectra from the cylindrically decaying Beer-Lambert law. (**E**) Comparison between experiment (solid lines) and expected decay (dashed lines) from the Beer-Lambert law at 765 and 800 nm. The experimental data are not in agreement with simple linear absorption, which suggests that additional processes, such as photon recycling, maintain substantial photon intensity at large distances.

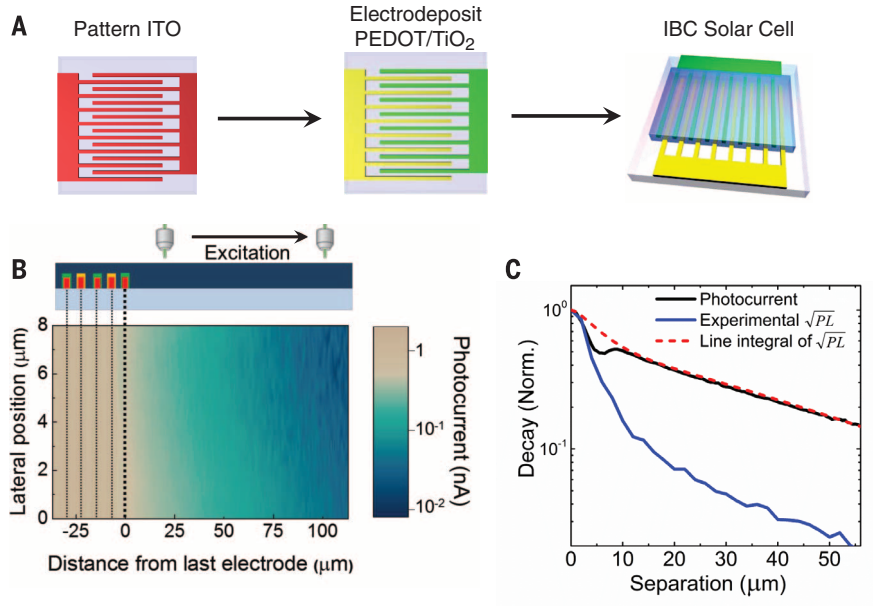

Fig. 2. Photocurrent mapping of an interdigitated back-contact (IBC) perovskite solar cell. (**A**) Fabrication process of the IBC device: (left) pattern a flat sheet of ITO, (middle) electrodeposit TiO_2 on half of the "fingers" and PEDOT on the other half, and (right) spin-coat the photoactive perovskite layer. (**B**) Photocurrent map at the edge of the active area of an IBC perovskite device. The lateral position is along the electrode direction. We observed photocurrent several tens of micrometers beyond the last electrode (*x*-axis position 0 μm, bold dashed line). (**C**) Comparison between normalized spatial decay of the photocurrent and square root of PL. These results suggest that photon densities, which propagate over large distances through the material assisted by photon recycling, can be extracted as photocurrent.

long-wavelength photons were absorbed and generated electron-hole (e^--h^+) pairs far from the original excitation spot. When these e^--h^+ pairs recombined, they regenerated the original emission spectrum that peaks near 765 nm, giving rise to the second observed peak. The photon energy gain between absorption and re-emission occurred via phonon-assisted thermalization.

With the observed spatial decay of photon intensity, charges are expected to be generated at comparable distances. To measure the spatial charge distribution directly, we designed a lateral solar cell with electron- and hole-selective electrodes. The fabrication process of this back-contacted device (Fig. 2A) began with a plain sheet of indium tin oxide (ITO) covering a glass substrate. Photolithography was used to make a pattern of ITO with interdigitated electrodes. The channel and electrode width was ~4 μm (a pitch of 8 μm). Electrodeposition was used to selectively deposit electron- and hole-blocking layers. On half of the electrodes, TiO_2 was deposited from a solution of $Ti(O_2)SO_4$, and poly-3,4-ethylenedioxythiophene (PEDOT) from a 3,4-ethylenedioxythiophene monomer-based solution was deposited in the remaining electrode surface. The TiO_2 layer was formed by hydrolysis, whereas the PEDOT film formed by polymerization under an external bias. Finally, a layer of perovskite was spin-coated from a standard precursor solution based on methylammonium iodide mixed with lead acetate in *N*,*N*′-dimethylformamide (*23*), and uniform film formation was detected on both electrodes [see supplementary materials and methods (*21*)].

The electric response of this device measured in the dark revealed a diode-like rectifying behavior. Under solar irradiation, a photovoltaic response with an open-circuit voltage of 0.5 V was observed (fig. S14), showing effective carrier selectivity at the electrodes. Photocurrent extraction appeared to be limited in our device compared with vertical solar cells, possibly due to energy barriers at the electrodes and an unfavorable charge collection geometry. For comparison, a lateral solar cell without selective layers (fig. S15) (*21*) showed a reduced charge selectivity, as well as very limited voltage and photocurrent.

We used confocal microscopy to map the spatially resolved photocurrent generation in these devices with an excitation resolution below 1 μm. The photocurrent probed the number of photoexcited carriers that reached the electrodes. Figure 2B shows a spatial map of photocurrent, both across the interdigitated electrodes (≤1 μm) and for photoexcitation beyond the electrodes (0 to 100 μm). The very slow falloff in photocurrent for excitation beyond the edge of the electrode structure (see also Fig. 2C) extends well beyond the reported diffusion lengths of lead halide perovskite thin films.

In the range of excitation fluences used in our experiment, PL in perovskites mainly arises from bimolecular recombination of charge carriers with volume density n (i.e., $PL \propto n^2$), consistent with e^--h^+ recombination (*10*, *24*). Hence, we can relate the locally generated PL, taken around the PL emission peak (765 nm), with the local charge density, and $\sqrt{PL} \propto n$ is a probe of the spatial charge distribution. Because $\sqrt{PL}$ decays cylindrically, it must be geometrically corrected by performing a line integral of $\sqrt{PL}$ over the length of the electrode, to compare it with the photocurrent measurements.

In Fig. 2C, we compare the decay of the integrated $\sqrt{PL}$ with the measured spatial decay of the photocurrent. We observed a similar decay in photocurrent and integrated $\sqrt{PL}$ beyond 8 μm, which is the resolution set by the electrode geometry. The agreement between these two quantities indicates that the red-shifted component of the recycled photons allows excitation transport over long distances, beyond carrier diffusion lengths, which eventually can be extracted as photocurrent from a solar cell.

To model this, we set up and solved a system of cylindrically symmetric partial differential equations based on existing theoretical approaches for photon recycling (*25*–*27*). We expanded these concepts (*21*) to account for local excitation and calculate the local photon distribution in the film

$$\frac{dn}{dt} = D\nabla^2 n + G + \frac{c}{n_s}\sum_{\lambda}\alpha_\lambda\gamma_\lambda - k_1 n - k_2 n^2 \quad (2)$$

$$\frac{d\gamma_\lambda}{dt} = D_\lambda\nabla^2\gamma_\lambda - \frac{c}{n_s}\alpha_\lambda\gamma_\lambda + (k_2 n^2 P_{stay})P_\lambda \quad (3)$$

The charge-carrier concentration n and the photon density γ were modeled (at different wavelengths λ) as a function of distance from the excitation spot. Input parameters are reported experimental values for carrier diffusion [diffusion constant D = 0.5 $cm^2\ s^{-1}$ (*9*, *11*, *12*)], mono- and bimolecular recombination rates of carriers [$k_1 = 10^6\ s^{-1}$ and $k_2 = 10^{-10}\ cm^3\ s^{-1}$; from our own measurements and (*10*, *28*)], and the measured wavelength-dependent absorption coefficients α_λ (Fig. 1C). (Additionally, t is time, G is the generation rate, c is the speed of light, n_s is the refractive index, P_{stay} is the optical probability of photon escape, and P_λ is the probability that light will be emitted with a given wavelength.) The experimentally measured external bimolecular rate had to be adjusted to account for photon recycling (*29*, *30*). All absorption of photons is assumed to result in the creation of e^--h^+ pairs, but only the bimolecular channel is radiative (with the spectrum as shown in Fig. 1C), and a proportion 1-P_{stay} [modeled to be 12.5% (*21*)] of these photons is lost through optical transmission out of the perovskite at the interfaces. The external PL quantum efficiency (PLQE) results from multiple internal recycling events and is related to the internal PLQE by the geometric series

$$PLQE_{ext} = \sum_{r=1}^{\infty}(PLQE_{int})^r(1 - P_{escape})^{r-1}P_{escape} = \frac{PLQE_{int}P_{escape}}{1 - PLQE_{int}(1 - P_{escape})} \quad (4)$$

The external PLQE varies with distance from the excitation spot and the carrier density (Fig. 3A). Photon recycling could be very efficient near the excitation spot but dropped off at larger distances for which charge-carrier densities are smaller. From Eq. 4, we find that internal PLQEs can exceed 50% for 1-sun illumination (here, sun is defined as the solar spectrum standard ASTM G173) (internal carrier density ~10^{15} cm^{-3}), corresponding to lower measured external PLQEs of ~10%. The observed recycling effect on extraction would be increased in a solar cell with homogenous illumination, which produces constant carrier densities over the full active area.

In order for this model to match the experimental photocurrent, recycling must be taken into account to explain the observed long spatial decays (Fig. 3B). On average, the model predicts one recycling event per photoexcited charge carrier under 1-sun illumination before the carrier decays

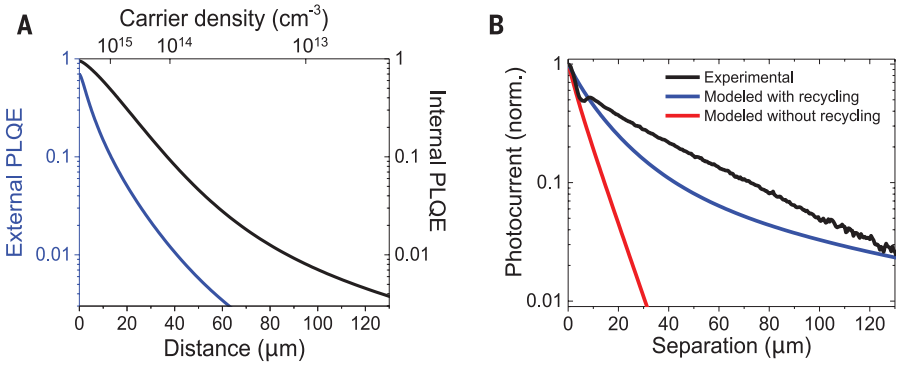

Fig. 3. Predicted effects of photon recycling. (**A**) Change in external and internal PLQE as a function of distance derived from a photon recycling diffusion model as presented in the text, with reported mono- and bimolecular recombination ($k_{mono} = 10^6\ s^{-1}$, $k_{bi} = 10^{-10}\ cm^3\ s^{-1}$) and diffusion constants (D = 0.5 $cm^2\ s^{-1}$) of photoexcited carriers. (**B**) Predicted spatial photocurrent decay for the model with and without photon recycling.

nonradiatively [calculation in the supplementary materials (*21*)] in a perovskite film in air on glass. This value relates to a photon recycling–assisted average excitation travel distance of 20 μm (fig. S18). The average travel distance could be enhanced at larger charge densities (for example, under high fluences) and can reach values beyond 50 μm.

In terms of e^--h^+ transport, our results suggest that the average distance a charge carrier can travel in a perovskite is not limited by the charge-carrier diffusion length, for as long as recombination is radiative and the photon stays in the film, the e^--h^+ pair can be regenerated and can propagate over large distances. This process creates a distinction between extraction and charge diffusion lengths and allows us to solve the existing contradiction of reported high recombination rates and long diffusion lengths.

What are the implications of the observations presented here for standard thin-film perovskite solar cells (*3*, *6*)? The thin-film samples from our work provide valuable model systems for these structures. Using the model and parameters developed above, we estimate that, under open-circuit conditions, in a device with a thickness of 350 nm and nonquenching electrodes, recycling produces a doubling of the internal photon density under 1-sun illumination. These effects can be enhanced further by minimizing nonradiative decay channels and being subjected to higher fluences, such as in solar concentrators, where high bimolecular recombination rates dominate. In the ideal case of unity PLQE and a perfect back mirror, photon recycling can produce internal photon densities up to 25 suns ($4n^2$ with n = 2.5) (*31*) in perovskite solar cells under open-circuit conditions. Photon management, such as the use of highly reflective back mirrors to minimize photonic losses and texturing of the top surface, offers promising approaches for using photon recycling to improve photoconversion efficiencies of perovskite solar cells toward the Shockley-Queisser limit. Higher photon densities lead to higher internal luminescence and a build-up of excited charges, which increase the split of quasi-Fermi levels and enhance the achievable open-circuit voltage in a solar cell.

REFERENCES AND NOTES

1. A. Kojima, K. Teshima, Y. Shirai, T. Miyasaka, *J. Am. Chem. Soc.* **131**, 6050–6051 (2009).
2. J.-H. Im, C.-R. Lee, J.-W. Lee, S.-W. Park, N.-G. Park, *Nanoscale* **3**, 4088–4093 (2011).
3. M. M. Lee, J. Teuscher, T. Miyasaka, T. N. Murakami, H. J. Snaith, *Science* **338**, 643–647 (2012).
4. M. Liu, M. B. Johnston, H. J. Snaith, *Nature* **501**, 395–398 (2013).
5. H.-S. Kim *et al.*, *Sci. Rep.* **2**, 591 (2012).
6. N. J. Jeon *et al.*, *Nature* **517**, 476–480 (2015).
7. J. Burschka *et al.*, *Nature* **499**, 316–319 (2013).
8. S. De Wolf *et al.*, *J. Phys. Chem. Lett.* **5**, 1035–1039 (2014).
9. C. Wehrenfennig, G. E. Eperon, M. B. Johnston, H. J. Snaith, L. M. Herz, *Adv. Mater.* **26**, 1584–1589 (2014).
10. F. Deschler *et al.*, *J. Phys. Chem. Lett.* **5**, 1421–1426 (2014).
11. Q. Dong *et al.*, *Science* **347**, 967–970 (2015).
12. D. Shi *et al.*, *Science* **347**, 519–522 (2015).
13. G. Xing *et al.*, *Science* **342**, 344–347 (2013).
14. S. D. Stranks *et al.*, *Science* **342**, 341–344 (2013).
15. E. Yablonovitch, O. D. Miller, S. R. Kurtz, in *Conference Record of the 38th IEEE Photovoltaic Specialists Conference*, Austin, TX, 3 to 8 June 2012 (IEEE, 2012), pp. 1556–1559.
16. L. S. Mattos *et al.*, in *Conference Record of the 38th IEEE Photovoltaic Specialists Conference*, Austin, TX, 3 to 8 June 2012 (IEEE, 2012), pp. 3187–3190.
17. O. D. Miller, E. Yablonovitch, S. R. Kurtz, *IEEE J. Photovoltaics* **2**, 303–311 (2012).
18. E. Dupont, H. C. Liu, M. Buchanan, S. Chiu, M. Gao, *Appl. Phys. Lett.* **76**, 4 (2000).
19. A. Sadhanala *et al.*, *J. Phys. Chem. Lett.* **5**, 2501–2505 (2014).
20. C. Wehrenfennig, M. Liu, H. J. Snaith, M. B. Johnston, L. M. Herz, *J. Phys. Chem. Lett.* **5**, 1300–1306 (2014).
21. Full details can be found in the supplementary materials on *Science* Online.
22. I. Suárez, E. J. Juárez-Pérez, J. Bisquert, I. Mora-Seró, J. P. Martínez-Pastor, *Adv. Mater.* **27**, 6157–6162 (2015).
23. W. Zhang *et al.*, *Nat. Commun.* **6**, 6142 (2015).
24. Y. Yamada, T. Nakamura, M. Endo, A. Wakamiya, Y. Kanemitsu, *J. Am. Chem. Soc.* **136**, 11610–11613 (2014).
25. J. L. Balenzategui, A. Martí, *Sol. Energy Mater. Sol. Cells* **90**, 1068–1088 (2006).
26. S. M. Durbin, J. L. Gray, *IEEE Trans. Electron. Dev.* **41**, 239–245 (1994).
27. R. Graaff, J. J. Ten Bosch, *Opt. Lett.* **25**, 43–45 (2000).
28. M. B. Johnston, L. M. Herz, *Acc. Chem. Res.* **49**, 146–154 (2016).
29. R. K. Ahrenkiel *et al.*, *Appl. Phys. Lett.* **55**, 1088–1090 (1989).
30. P. Renaud, F. Raymond, B. Bensaïd, C. Vèrié, *J. Appl. Phys.* **71**, 1907–1913 (1992).
31. Q. Lin, A. Armin, R. C. R. Nagiri, P. L. Burn, P. Meredith, *Nat. Photonics* **9**, 106–112 (2014).

ACKNOWLEDGMENTS

We acknowledge financial support from the Engineering and Physical Sciences Research Council of the UK (EPSRC) and King Abdulaziz City for Science and Technology. L.M.P.-O. thanks the Cambridge Home European Scheme for financial support. L.M.P.-O. and H.J.B. also thank the Nano Doctoral Training Center (NanoDTC) of the EPSRC for financial support. M.S., M.V., and J.M.R. thank the Winton Programme for the Physics of Sustainability (University of Cambridge). M.C.-Q. would like to thank the Marie Curie Actions (FP7-PEOPLE-IEF2013) for funding. M.A. acknowledges financial support from the President of the UAE's Distinguished Student Scholarship Program (DSS), granted by the UAE's Ministry of Presidential Affairs. M.A.-J. thanks Nyak Technology Limited for a Ph.D. scholarship. B.E. acknowledges the Foundation for Fundamental Research on Matter (FOM), which is part of the Netherlands Organisation for Scientific Research (NWO). F.D. acknowledges funding from a Herchel Smith Research Fellowship. We thank H. Sirringhaus, N. Greenham, U. Steiner, E. Reisner, and R. Phillips for providing support and access to their facilities. Experimental data are available at www.repository.cam.ac.uk/handle/1810/253689.

SUPPLEMENTARY MATERIALS

www.sciencemag.org/content/351/6280/1430/suppl/DC1
Materials and Methods
Supplementary Text
Figs. S1 to S19
References (*32*–*46*)

22 December 2015; accepted 2 February 2016
10.1126/science.aaf1168

ECONOMICS

Evaluating replicability of laboratory experiments in economics

Colin F. Camerer,[1]*† Anna Dreber,[2]† Eskil Forsell,[2]† Teck-Hua Ho,[3,4]† Jürgen Huber,[5]† Magnus Johannesson,[2]† Michael Kirchler,[5,6]† Johan Almenberg,[7] Adam Altmejd,[2] Taizan Chan,[8] Emma Heikensten,[2] Felix Holzmeister,[5] Taisuke Imai,[1] Siri Isaksson,[2] Gideon Nave,[1] Thomas Pfeiffer,[9,10] Michael Razen,[5] Hang Wu[4]

The replicability of some scientific findings has recently been called into question. To contribute data about replicability in economics, we replicated 18 studies published in the *American Economic Review* and the *Quarterly Journal of Economics* between 2011 and 2014. All of these replications followed predefined analysis plans that were made publicly available beforehand, and they all have a statistical power of at least 90% to detect the original effect size at the 5% significance level. We found a significant effect in the same direction as in the original study for 11 replications (61%); on average, the replicated effect size is 66% of the original. The replicability rate varies between 67% and 78% for four additional replicability indicators, including a prediction market measure of peer beliefs.

The deepest trust in scientific knowledge comes from the ability to replicate empirical findings directly and independently. Although direct replication is widely applauded (*1*), it is rarely carried out in empirical social science. Replication is now more important than ever, because the quality of results has been questioned in many fields, such as medicine (*2*–*5*), neuroscience (*6*), and genetics (*7*, *8*). In economics, concerns about inflated findings in empirical (*9*) and experimental analyses (*10*, *11*) have also been raised. In the social sciences, psychology has been the most active in both self-diagnosing the forces that create "false positives" and conducting direct replications (*12*–*15*). Several high-profile replication failures (*16*, *17*) quickly led to changes in journal publication practices (*18*). The recent Reproducibility Project: Psychology (RPP) replicated 100 original studies published in three top journals in psychology. The vast majority (97) of the original studies reported "positive findings," but in the replications, the RPP only found a significant effect in the same direction for 36% of these studies (*19*).

In this report, we provide insights into the replicability of laboratory experiments in economics. Our sample consists of all 18 between-subject laboratory experimental papers published in the *American Economic Review* and the *Quarterly Journal of Economics* between 2011 and 2014. The most important statistically significant finding,

Science
AAAS

Photon recycling in lead iodide perovskite solar cells

Luis M. Pazos-Outón, Monika Szumilo, Robin Lamboll, Johannes M. Richter, Micaela Crespo-Quesada, Mojtaba Abdi-Jalebi, Harry J. Beeson, Milan Vrucinic, Mejd Alsari, Henry J. Snaith, Bruno Ehrler, Richard H. Friend and Felix Deschler (March 24, 2016)
Science **351** (6280), 1430-1433. [doi: 10.1126/science.aaf1168]

Editor's Summary

Perovskite solar cells recycle photons

Inorganic-organic perovskite solar cells are very efficient in part because the charge carriers exhibit very long path lengths. Pazos-Outón *et al.* show that photon recycling, as seen previously in highly efficient gallium arsenide solar cells, contributes to this effect (see the Perspective by Yablonovitch). In most solar cells, the recombination of photogenerated charge carriers (electrons and holes) wastes all of the energy. In these lead tri-iodide cells, recombination emits a photon that can be reabsorbed and create more charge carriers.

Science, this issue p. 1430; see also p. 1401

Science (print ISSN 0036-8075; online ISSN 1095-9203) is published weekly, except the last week in December, by the American Association for the Advancement of Science, 1200 New York Avenue NW, Washington, DC 20005.